miR-183/96 plays a pivotal regulatory role in mouse photoreceptor maturation and maintenance

Lue Xiang[a,b,1], Xue-Jiao Chen[a,b,1], Kun-Chao Wu[a,b], Chang-Jun Zhang[a,b], Gao-Hui Zhou[a,b], Ji-Neng Lv[a,b], Lan-Fang Sun[a,b], Fei-Fei Cheng[a,b], Xue-Bi Cai[a,b], and Zi-Bing Jin[a,b,2]

[a]Laboratory for Stem Cell and Retinal Regeneration, Institute of Stem Cell Research, Division of Ophthalmic Genetics, The Eye Hospital, Wenzhou Medical University, Wenzhou 325027, China and [b]State Key Laboratory of Ophthalmology, Optometry, and Vision Science, Wenzhou 325027, China

Edited by Jeremy Nathans, Johns Hopkins University, Baltimore, MD, and approved April 26, 2017 (received for review November 22, 2016)

MicroRNAs (miRNAs) are known to be essential for retinal maturation and functionality; however, the role of the most abundant miRNAs, the miR-183/96/182 cluster (miR-183 cluster), in photoreceptor cells remains unclear. Here we demonstrate that ablation of two components of the miR-183 cluster, miR-183 and miR-96, significantly affects photoreceptor maturation and maintenance in mice. Morphologically, early-onset dislocated cone nuclei, shortened outer segments and thinned outer nuclear layers are observed in the miR-183/96 double-knockout (DKO) mice. Abnormal photoreceptor responses, including abolished photopic electroretinography (ERG) responses and compromised scotopic ERG responses, reflect the functional changes in the degenerated retina. We further identify Slc6a6 as the cotarget of miR-183 and miR-96. The expression level of Slc6a6 is significantly higher in the DKO mice than in the wild-type mice. In contrast, Slc6a6 is down-regulated by adeno-associated virus-mediated overexpression of either miR-183 or miR-96 in wild-type mice. Remarkably, both silencing and overexpression of Slc6a6 in the retina are detrimental to the electrophysiological activity of the photoreceptors in response to dim light stimuli. We demonstrate that miR-183/96–mediated fine-tuning of Slc6a6 expression is indispensable for photoreceptor maturation and maintenance, thereby providing insight into the epigenetic regulation of photoreceptors in mice.

miR-183/96/182 cluster | regulation | photoreceptor | taurine transporter | degeneration

MicroRNAs (miRNAs) are known to act as important epigenetic coordinators during posttranscriptional processing via the regulation of hundreds of target genes with great temporal and spatial precision (1–3). Wholesale and individual disruption of miRNAs has been shown to result in various retinal defects and other sensorial diseases (4–6). The retinal photoreceptor is a type of ciliated neuron in which the miR-183 cluster represents the most highly expressed miRNAs. Although different mouse models have been generated to determine the roles of the miR-183 cluster, many previous studies have used nonspecific or incomplete miRNA depletion to examine the effects of eliminating specific miRNAs on photoreceptor degeneration (5, 6). Little is known about the impact of a "null" miR-183/96/182 model in vivo.

A recent study of miR-182 and miR-183 identified these two miRNAs as essential for the maturation and function of cone photoreceptors (7). In addition, their expression is necessary and sufficient for the formation of cone outer segments (OSs) (7). Another study likewise showed that inactivation of the miR-183 cluster by gene trapping resulted in abnormal electroretinography (ERG) responses, progressive synaptic defects, and progressive retinal degeneration (4). Other investigators have reported that impairment of miR-96 resulted in hair cell death in the inner ear, as well as progressive hearing loss in zebrafish, mice, and humans (8–10). Notwithstanding these findings, however, our understanding of the regulatory mechanism of the miR-183 cluster in the retina remains fragmented, even with a recent investigation demonstrating that this miRNA cluster controls the retinal architecture during development (11).

It has been reported that miR-96 may be involved in the pathogenesis of multiple system atrophy (MSA) by interacting with Slc6a6 (12). Slc6a6, a taurine transporter, is highly expressed in ciliated cells (13, 14). In diseased retinas, Slc6a6 acts as a neuronal protectant by regulating several "essential genes" of the photoreceptors via the retinal long noncoding RNA Tug1 to protect the photoreceptors from degeneration (15). It has been shown that mice deficient in Slc6a6 exhibit progressive degeneration of the outer nuclear layers (ONLs) from postnatal day (P) 14 onward (16); however, whether the overexpression of Slc6a6 in the retina is harmful to photoreceptors is not known.

We previously reported that no significant structural changes appeared in miR-182 knockout (KO) mice (17). Because miR-182, miR-183, and miR-96 are transcribed simultaneously in a polycistronic manner, we asked whether miR-183/96 could compensate for the lack of miR-182. To address this question, we generated double-KO (DKO) mice, and found that depletion of both miR-183 and miR-96 could lead to defective cone nuclear polarization and progressive retinal degeneration. Using these DKO mice, we found that miR-183/96 balances the expression of genes that are essential for photoreceptors by precisely controlling Slc6a6, which is indispensable for the proper development and function of mouse photoreceptors.

Results

Simultaneous Ablation of miRNA-183 and miRNA-96 in Mice. The miR-183/96/182 host *mirc35hg* is located on mouse Chr6qA3.3, which spans >15 kb. It is a polycistronic gene from which miR-183, miR-96, and miR-182 are transcribed. In this study, we used a conventional knockout strategy to generate an miR-183/96 DKO mouse model to separately assess the function of these two

Significance

The polycistronic miR-183/96/182 cluster is highly expressed in various types of terminally differentiating sensory neurons, including photoreceptors. Although miR-182 single-knockout mice do not exhibit significant retinal architecture alterations in photoreceptors, deletion of miR-183 and miR-96 gives rise to severe defects in cone maturation. Long-term follow-up analysis reveals that miR-183/96 ablation results in progressive photoreceptor degeneration. Mechanistic studies demonstrate that miR-183 and miR-96 directly regulate the expression of the taurine transporter Slc6a6. The expression levels of photoreceptor-specific genes change in accordance with the knockdown or overexpression of Slc6a6 in vivo. In both cases, the mouse scotopic electroretinography responses are compromised. Our findings reveal that the epigenetic regulation of miR-183/96 via Slc6a6 is essential for mouse photoreceptor formation and functionalization.

Author contributions: L.X. and Z.-B.J. designed research; L.X., X.-J.C., K.-C.W., C.-J.Z., G.-H.Z., J.-N.L., L.-F.S., F.-F.C., and X.-B.C. performed research; X.-J.C., C.-J.Z., G.-H.Z., and F.-F.C. analyzed data; and L.X. and Z.-B.J. wrote the paper.

The authors declare no conflict of interest.

This article is a PNAS Direct Submission.

Freely available online through the PNAS open access option.

[1]L.X. and X.-J.C. contributed equally to this work.

[2]To whom correspondence should be addressed. Email: jinzb@mail.eye.ac.cn.

This article contains supporting information online at www.pnas.org/lookup/suppl/doi:10.1073/pnas.1618757114/-/DCSupplemental.

www.pnas.org/cgi/doi/10.1073/pnas.1618757114

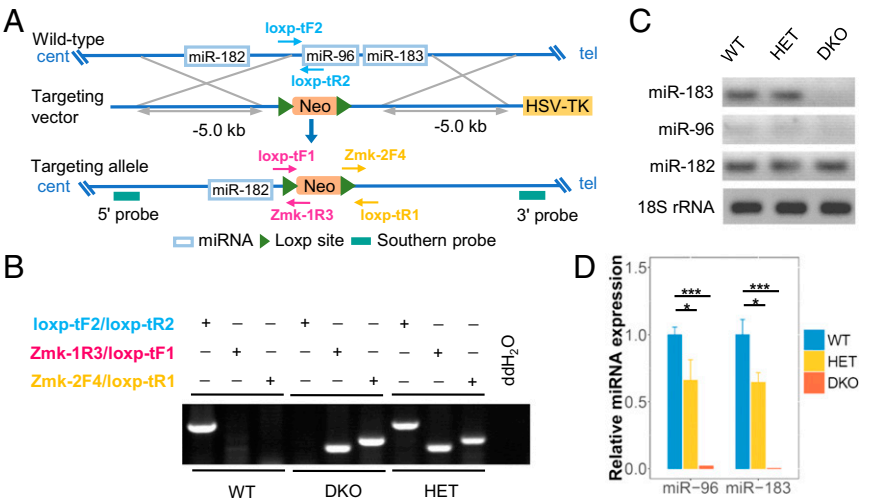

Fig. 1. Generation of miR-183/96 DKO mice. (*A*) A conventional knockout strategy was used to generate the DKO mice. The neomycin resistance gene was preserved in the DKO mice. Neo, neomycin; tel, telomeric; cent, centromeric. (*B*) Genotyping strategy for the WT mice and DKO mutants. (*C* and *D*) RT-PCR (*C*) and qRT-PCR (*D*) analysis of miR-183/96/182 expression at P90. Relative expression levels of microRNAs are normalized to the level of U6. The normalized values represent mean ± SEM. $n = 3$. $^{*}P < 0.05$, $^{***}P < 0.001$ between the DKO mice and their littermates, Student's *t* test.

miRNAs without interfering with miR-182. A targeting vector carrying a neomycin cassette was designed to replace a 2.085-kb region that included pre–miR-183 and pre–miR-96 (Fig. 1*A* and *SI Appendix*, Fig. S1 *A*–*C*).

To generate miR-183/96 DKO mice, primer pairs capable of distinguishing homozygous mutants from the heterozygotes and wild-type (WT) mice were designed for genotyping (Fig. 1 *A* and *B*). miRNA expression was validated by RT-PCR and quantitative RT-PCR (qRT-PCR). Our knockout approach was successful, as demonstrated by the absence of miR-183 and miR-96 in the DKO mice (Fig. 1 *C* and *D*). Accordingly, the expression of these two miRNAs was reduced to 64.4% and 66%, respectively, in the

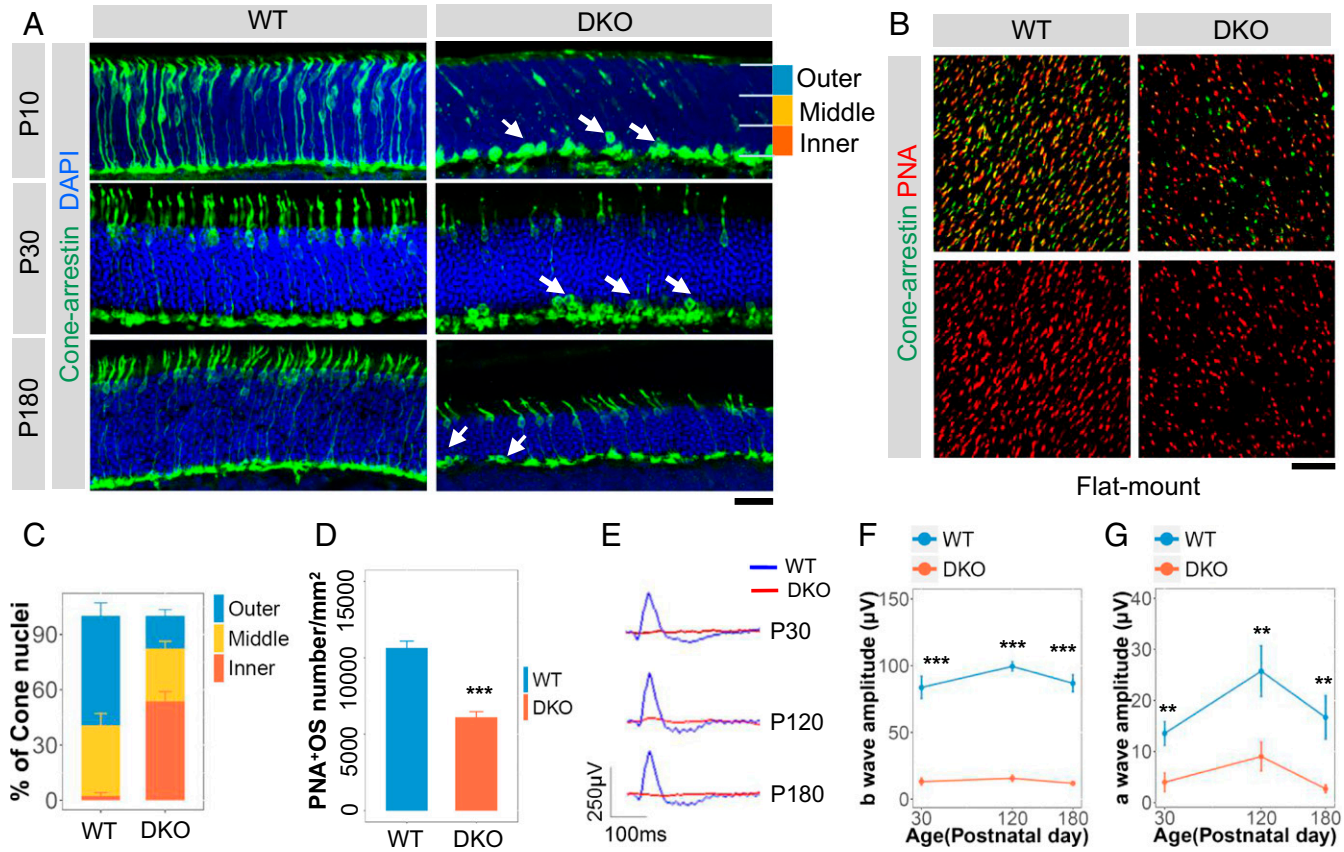

Fig. 2. Depletion of miR-183/96 results in early-onset defects in nuclear polarization and shortened OSs of cones and abolished ERG in mice. (*A*) Cone arrestin immunostaining at P10, P30, and P180 in WT (*Left*) and DKO (*Right*) mouse retinas. White arrows point to cone nuclei located at the basal part of the ONL. (Scale bar: 20 μm.) (*B*) Flat retinal whole-mount immunostaining of PNA and cone arrestin at P10. (*C*) The number of cone nuclei on the outer, middle, and inner areas of the ONL shown in *A* at P10; $n = 4$. (*D*) Quantification of the PNA-positive OSs per mm^2 as shown in *B*. $n = 4$. (*E*) Representative photopic ERG recordings of the DKO and WT mice at P30, P120, and P180. (*F*–*G*) Comparison of the b-wave amplitudes (*F*) and *a*-wave amplitudes (*G*) between the DKO mice and age-matched WTs. $n = 4$, 3, and 3 for photopic responses of mice at P30, P120, and P180, respectively. In *C*–*G*, the normalized values represent mean ± SEM. $^{**}P < 0.005$, $^{***}P < 0.001$, Student's *t* test.

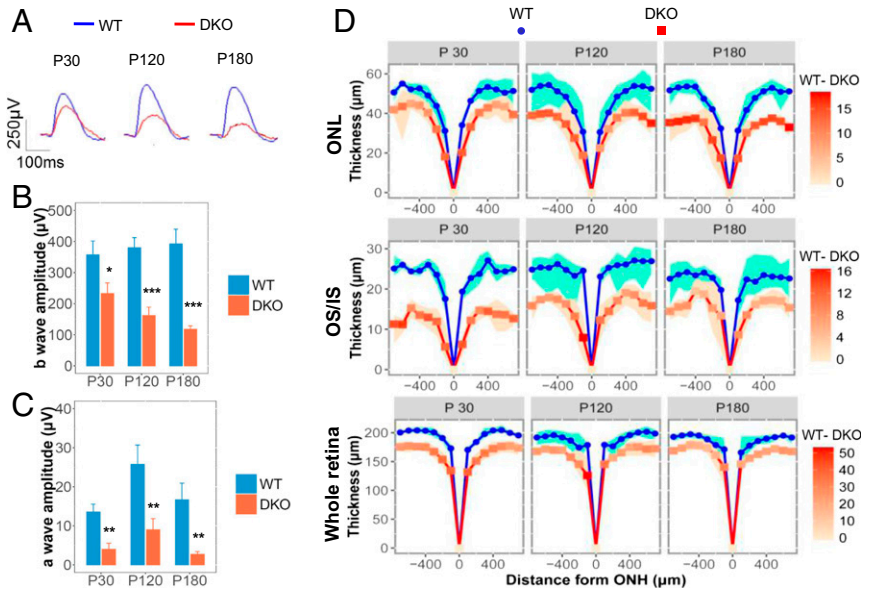

Fig. 3. Ablation of miR-183/96 causes progressive retinal degeneration. (*A*) Representative scotopic ERG recordings of DKO and WT mice. (*B* and *C*) b-wave (*B*) and a-wave (*C*) amplitudes for the DKO mice and age-matched controls. $n = 4$, 3, and 4 for scotopic responses in mice at P30, P120, and P180, respectively. The normalized values represent mean ± SEM. $*P < 0.05$, $**P < 0.005$, $***P < 0.001$ between the DKO mice and age-matched controls, Student's t test. (*D*) Quantification of the thickness of the ONL, OS/IS, and whole retina from SD-OCT images of mice at P30–P180. The red intensities on the curve of the DKO mice represent the thickness of the WT sample minus that in the DKO sample. Blue and red indicate the minimum and maximum thickness, respectively, in the WT and DKO samples at each point. $n = 4$ for each group.

heterozygous mice (Fig. 1 *C* and *D*). On the contrary, in the WT mice, the expression levels of the miR-183 cluster and photoreceptor-specific genes increased sharply from P1 to P14, indicating that miR-183/96 may be involved in photoreceptor maturation in mice (*SI Appendix*, Fig. S2 *A* and *B*).

Depletion of miR-183/96 Leads to Abnormal Development of Cones. We first surveyed the potential architectural defects in the retinas of DKO mice. Staining of the retinal pigment epithelium cells, bipolar cells, horizontal cells, and ganglion cells with selected cell type-specific antibodies revealed no obvious abnormalities in these cell populations in the DKO mice at P21 (*SI Appendix*, Figs. S3–S5).

Intriguingly, immunostaining for cone arrestin revealed that the cones in miR-183/96–deficient mice exhibited impaired nuclear polarization during development (Fig. 2*A*). We found that 53.6% of the cone nuclei had retracted to the inner part rather than to the outer part of the ONL at P10 (Fig. 2*C*). In addition, at P180, cones that did not undergo correct polarization remained in the basal part of the ONL (Fig. 2*A*). To better understand these cone defects during development, we performed immunostaining for peanut agglutinin lectin (PNA) at P10, by which time the outer plexiform layer (OPL) had formed. Examination of whole-mount preparations revealed markedly shortened OSs of the cones in the DKO mice (Fig. 2 *B* and *D*); therefore, we concluded that the absence of miR-183/96 results in early-onset polarization defects and shorter OSs of cones.

Depletion of miR-183/96 Leads to Abolished Photopic ERG Responses and Progressively Attenuated Scotopic ERG Responses. Because ERG is widely used for evaluating light responses of photoreceptors, we subjected the miR-183/96 DKO mice to ERG at P30, P90, and P180. At P30, the earliest evaluation time point, the miR-183/96 DKO mice displayed abolished photopic ERG responses lacking a-waves and b-waves, which did not recover in the adult mice at P120 and P180 (Fig. 2 *E*–*G*). This manifestation correlates with the nuclear mislocalization and defective OS formation observed in cones.

To investigate whether miR-183 and miR-96 affect rod function, we assessed the responsiveness of the miR-183/96 DKO mouse retinas to dim light stimuli. The miR-183/96–deficient mice showed progressively attenuated scotopic responses, with b-wave amplitudes decreasing from 65.3% at P30 to 30.3% at P180 compared with those in the WT controls (Fig. 3 *A* and *B*). The a-wave amplitudes were diminished in the DKO mice as well (Fig. 3*C*).

Depletion of miR-183/96 Leads to Thinned ONLs, Activated Microglia, and Thinner Blood Vessels. We also measured outer retinal thickness by spectral domain optical coherence tomography (SD-OCT), a noninvasive technique that enables visualization of changes in retinal thickness. Based on an assessment of the thickness of the ONL, inner segment (IS), and OS, as well as the entire retina from P30 to P180, we found that those anatomic structures were generally thinner in the DKO mice than in the WT mice (Fig. 3*D*). The inner nuclear layer (INL) appeared to be unaffected, however (*SI Appendix*, Fig. S6 *A* and *B*). The thickness of the ONL decreased progressively, suggesting photoreceptors as the primary cell type affected by the degeneration of retinas lacking miR-183/96. This result was validated by classical histological analyses (*SI Appendix*, Fig. S7 *A* and *B*).

To investigate microglial activity in our DKO model, we performed immunostaining for Iba1. It is well known that the microglia reside predominantly in the IPL and OPL and migrate toward the subretinal space under such disease conditions as retinitis pigmentosa (18–21). In the DKO mice, increased numbers of Iba1-positive cells were observed in the ONLs, indicating microglial activation (*SI Appendix*, Fig. S8 *A*–*C*); thus, we speculated that this activation may be involved in ONL thinning.

The OSs are highly metabolically active subcellular structures that require a constant blood supply. Thus, we used fundus fluorescein angiography (FFA) to measure the diameter of blood vessels in the DKO mice. Thinner blood vessels were observed in these mice at P30 and P120 (*SI Appendix*, Fig. S7 *C* and *D*).

Slc6a6 and Rnf217 Are the Two Most Potent Cotargets of miR-183 and miR-96. We investigated the underlying molecular mechanism of retinal degeneration in the absence of miR-183/96 in mice. To identify mutual candidates targeted by miR-183 and miR-96, we performed RNA-seq at P7 and P120. By screening the genes that were up-regulated from 2- to 15-fold by reads per kilobase per million mapped reads (RPKM) and overlapped with the predicted targets of miR-183 and miR-96 (www.targetscan.org/), we found that Slc6a6, Rnf217, Dmxl1, and Med1 were the four potential cotargets of miR-183 and miR-96 at P7 and P120, suggesting that these genes may be involved in retinal development as well as in visual function (*SI Appendix*, Fig. S9*A*). In a study of MSA, Slc6a6 was reported to be regulated by miR-96 (12). To verify the target genes, we conducted a luciferase assay with reporter plasmids consisting of the empty control, WT, or mutant 3′ UTR of Slc6a6, Rnf217, Dmxl1, and Med1 cotransfected with miR-183 and miR-96 mimics into HEK293 cells. As shown in *SI Appendix*, Fig. S9 *B*–*D*, Slc6a6, Rnf217, and Dmxl1 were strongly

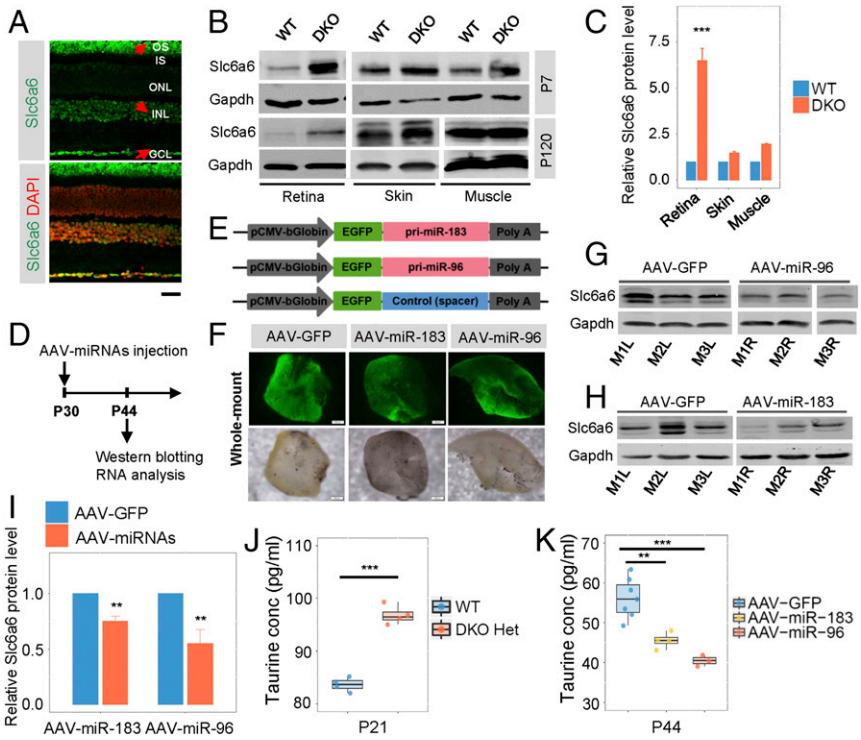

Fig. 4. Slc6a6 is a target of both miR-183 and miR-96 in the mouse retina. (*A*) Immunostaining reflects the endogenous expression of Slc6a6 in WT mouse retinas at P90. The red arrows point to cells with high expression. (Scale bar: 20 μm.) (*B*) Western blot verification of the expression of miR-183/96 target Slc6a6 in mouse tissues at P7 and P120. (*C*) Quantification of Slc6a6 protein level relative to Gapdh level at P7 shown in *B*. $n = 3$. (*D*) Schematic representation of the experiments. (*E*) AAV-based miR-183, miR-96, and control expression cassettes were driven by the pCMV-bGlobin promoter. (*F*) AAV-miR-183, AAV-miR-96, and their control vector were successfully expressed in retinas. (*G* and *H*) Slc6a6 was down-regulated in both miR-96 (*G*) and miR-183 (*H*) overexpressing WT retinas at P30. M1L, mouse 1 left eye; M1R, mouse 1 right eye, etc. (*I*) Quantification of Slc6a6 protein levels relative to GAPDH levels shown in *G* and *H*. $n = 4$. (*J* and *K*) The concentration of taurine was increased in the DKO heterozygous mice at P21 (*J*) and decreased in the WT mice overexpressing miR-183 or miR-96 at P44 (*K*). DKO Het, miR-183/96 DKO heterozygotes; conc, concentration. In *C*, and *I*–*K*, the normalized values represent mean ± SEM. Taurine concentrations are represented as median ± SEM. $^{**}P < 0.005$, $^{***}P < 0.001$, Student's *t* test.

regulated by miR-183. Slc6a6 and Rnf217 were also targeted by miR-96 (*SI Appendix*, Fig. S9 *B* and *C*). These results demonstrated that Slc6a6 and Rnf217 were the two most potent targets of these two miRNAs and that Med1 was not a target of either miR-183 or miR-96 (*SI Appendix*, Fig. S9 *B*–*E*).

Slc6a6 Is Regulated by miR-183 and miR-96 in Adolescent and Adult Mice. Slc6a6, also known as the taurine transporter, is highly expressed in ciliated cells (13, 14). As its name implies, Slc6a6 pumps taurine into cells and is critical for the development of vision and hearing and in skeletal muscles and the central nervous system (22–24). We found that Slc6a6 was widely expressed in the retina, including INL, ganglion cell layer (GCL), and photoreceptor OS. High expression of Slc6a6 was observed at both protein and RNA levels in WT photoreceptors (Fig. 4*A* and *SI Appendix*, Fig. S10*A*).

To assess Slc6a6 expression in vivo, Western blot analysis of P7 and P120 mouse retinas was performed. Our results showed that the levels of Slc6a6 proteins were increased in the DKO mice compared with that in the WT mice, suggesting that Slc6a6 is a target of miR-183/96. In addition, up-regulation of Slc6a6 was significant in the retina but not in nonneural tissues such as the skin or muscle (Fig. 4 *B* and *C* and *SI Appendix*, Fig. S10*B*). In contrast, the Slc6a6 protein was down-regulated by overexpression of miR-183 (decreased to 75.08%) or miR-96 (decreased to 55.36%) in WT retinas with adeno-associated virus (Fig. 4 *D*–*I*). Consistently, taurine levels were enhanced in the heterozygous retinas and were reduced in the presence of exogenous miR-183 or miR-96 in WT retinas (Fig. 4 *J* and *K*). In brief, these results collectively suggest that Slc6a6 is regulated by miR-183 and miR-96 in adolescent and adult mice.

Slc6a6 Is an Indispensable Factor in the Mouse Retina. To further assess the function of Slc6a6 in photoreceptors, we introduced AAV-Slc6a6 RNAi vector and its control carrying mCherry into WT mice at P30 (Fig. 5*A*). As expected, Slc6a6 expression in the retinas injected with AAV-Slc6a6 RNAi decreased to half that of the controls at P44 (Fig. 5*B*). Moreover, retinas with insufficient Slc6a6 showed degenerative features in the ONLs (Fig. 5*C*). The mouse eyes treated with AAV-Slc6a6 RNAi displayed attenuated ERG responses compared with that of the controls (Fig. 5*D*). In addition, the scotopic ERG responses were more significantly affected than the photopic ERG responses, indicating that the rods were much more sensitive to the absence of Slc6a6 expression than the cones. In addition, silencing of Slc6a6 led to an overall down-regulation of randomly-selected photoreceptor specific genes (Fig. 5*E* and *SI Appendix*, Fig. S11*A*). These observations validated the notion that Slc6a6 is necessary for the maintenance of photoreceptor structure and function.

Overexpression of Slc6a6 Is Detrimental to Mouse Photoreceptors. Slc6a6 transports taurine, which enhances the expression of several photoreceptor-specific genes (15). Previous studies have found that the overexpression of essential genes, such as Cngb1, Rom1, and Rho (25–27), can be detrimental to photoreceptors. We hypothesized that the overexpression of Slc6a6 is harmful to photoreceptors by the activation of essential genes. Therefore, we injected AAV-Slc6a6 and its controls into WT mice following the same procedures as for injection of AAV-Slc6a6 RNAi (Fig. 5*F*). The mean level of Slc6a6 mRNA was 14.37-fold higher in the AAV-Slc6a6–treated mouse retinas compared with the AAV-GFP–treated control retinas (Fig. 5*G*). Histological analyses revealed degeneration of the photoreceptors in response to the overabundance of Slc6a6 (Fig. 5*H*). Similar to the gene silencing experiments, overexpression of Slc6a6 mainly affected scotopic ERG responses (Fig. 5*I*). Interestingly, many of the essential genes expressed in rods and/or cones were up-regulated (Fig. 5*J* and *SI Appendix*, Fig. S11*B*). In particular, Cngb1 and Rom-1 were among the top three most greatly enhanced genes. However, screening the potential targets of the miR-183 cluster using TargetScan did not identify Cngb1 or Rom1 as a direct target of these three miRNAs. These findings validate our hypothesis that the overexpression of Slc6a6 is detrimental to mouse photoreceptors.

Discussion

Previous studies have reported that the down-regulation of expression of the miR-183 cluster in different models can lead to retinal degeneration (4–6). Although the retinal degeneration observed in our DKO mice was similar to that reported in previous models, the defects in the cones were distinct from those observed in other studies. In our study, impaired nuclear polarization of the cones was observed as early as P10, and photopic

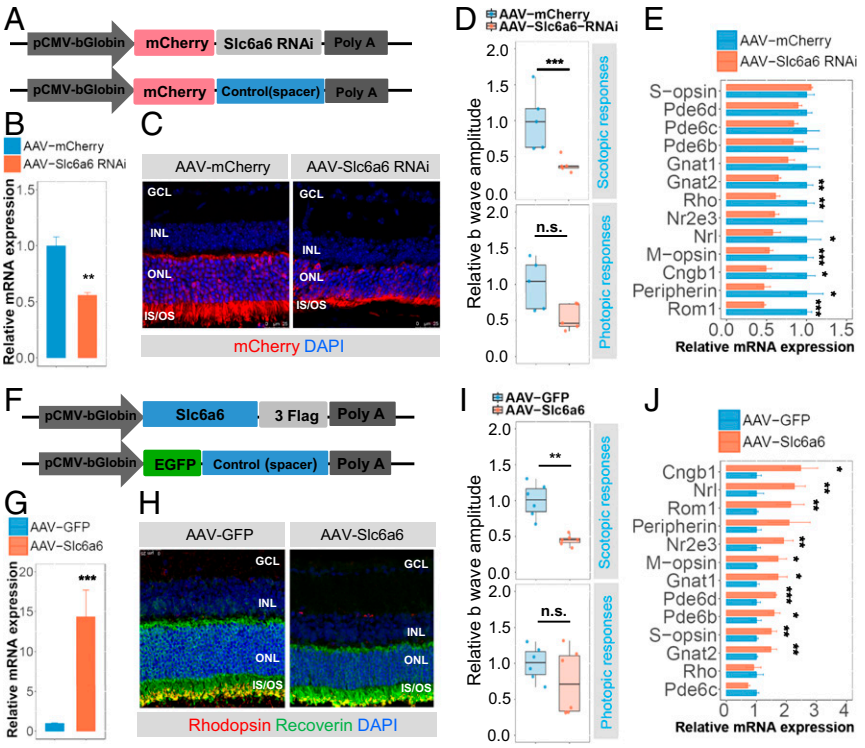

Fig. 5. Both silencing Slc6a6 and overexpressing Slc6a6 are detrimental to photoreceptors. (*A*) Slc6a6 RNAi sequences or spacer sequences were inserted downstream of mCherry into the AAV vectors. (*B*) qRT-PCR analysis of Slc6a6 expression in AAV-Slc6a6 RNAi-injected eyes compared with the control eyes. $n = 3$. (*C* and *H*) Retinas infected with AAV-Slc6a6 RNAi or AAV-Slc6a6 showed degenerative features in the photoreceptors. (*D* and *I*) Eyes injected with AAV-Slc6a6 RNAi or AAV-Slc6a6 displayed significantly attenuated scotopic ERG responses compared with the control eyes. $n = 5$ for AAV-Slc6a6 RNAi, $n = 6$ for AAV-Slc6a6 subretinal injection in mice. (*E*) Bar charts showing the general down-regulation of randomly-selected photoreceptor-specific genes. $n = 4$. (*F*) AAV-based Slc6a6 and control expression cassettes were driven by the pCMV-bGlobin promoter. (*G*) Slc6a6 expression in AAV-Slc6a6–injected retinas compared with the AAV-GFP–injected WT retinas assessed by qRT-PCR. $n = 3$. (*J*) Bar charts showing the general up-regulation of photoreceptor-specific genes. $n = 4$. In *B*–*J*, for the qRT-PCR bar plot, the normalized values represent mean ± SEM. For the ERG amplitude boxplot, the relative amplitudes are normalized to the mean amplitudes of control eyes; the normalized values represent median ± SEM. $*P < 0.05$; $**P < 0.005$; $***P < 0.001$; n.s., not significant, Student's *t* test.

ERG was abolished at P30 (Fig. 2 *A* and *E*). The ONL degenerated progressively, whereas the shortened IS/OS exhibited developmental retardation in the DKO mice. The disparity between P30 and P120 was reduced, indicating that maturation and degeneration occurred in parallel (Fig. 3*D*).

To investigate the function of each of the miRNAs in the miR-183 cluster, we generated a miR-182–depleted mouse model, which demonstrated that the outer retinal layer thickness remained relatively normal during development (17). Interestingly, when miR-183/96 was knocked out in mouse retinas, the photoreceptors were markedly affected, resulting in a polarization defect of the cones and photoreceptor degeneration (Figs. 2 and 3). Thus, miR-183/96 likely has a greater impact than miR-182 on the formation of photoreceptors. Although depletion of the most abundant miRNA in the cluster, miR-182, did not affect the morphogenesis of photoreceptors, the visual function of the miR-182 KO mice was not assessed. Furthermore, the effects of miR-183 and miR-96 on photoreceptor morphogenesis have not been investigated separately. It is possible that the defects observed in the DKO photoreceptors can be attributed to the combined or single action of the two miRNAs. Thus, determining which miRNA in the miR-183 cluster is the major contributor to the formation and development of photoreceptors merits evaluation.

Various transcriptional factors, such as Crx, facilitate the expression of opsin, which is essential for photoreceptor functions (28, 29). Interestingly, taurine, a known cysteine derivative, is transported by Slc6a6 into photoreceptors to enhance the expression of many essential genes (15); however, overexpression of two essential genes, Cngb1 and Rom1, has been reported to result in attenuated scotopic ERG and photopic ERG responses, respectively (25, 26). We found that the persistent expression of Slc6a6 resulted in an up-regulation of Cngb1 and Rom1, which may explain the attenuated ERG responses (Fig. 5). Of note, knocking down Slc6a6 in DKO mice partially restored the scotopic ERG responses (*SI Appendix*, Fig. S12 *A*–*E*). Nonetheless, the detrimental role of essential genes in DKO retinas may exemplify the broader Slc6a6-dependent undesirable side effects. Other downstream essential genes and miR-183/96 targets may contribute to the abnormalities observed in DKO mice as well.

Our mouse model also exhibited an unstable gait and circling behavior, accompanied by developmental retardation similar to that observed in the miR-183 cluster inactivation model (Movie S1) (4). The mice lost their balancing capability, went around in circles, and had difficulty staying still. These phenotypes were likely related to a defect in the vestibular system (30, 31). The buried food pellet test indicated that the olfactory function in these mice was affected as well (*SI Appendix*, Fig. S13) (32).

Taken together, our results demonstrate distinct retinal phenotypes arising from the depletion of miR-183/96 in mice. Photoreceptors are affected mainly by polarization defects and degeneration. The miR-183/96–mediated precise regulation of photoreceptor-specific genes via Slc6a6 is essential for photoreceptor maturation and maintenance. Our findings provide valuable insight into the epigenetic modulation of photoreceptors based on the miR-183/96 DKO model.

Methods

Animals. The miR-183/96 DKO mice, Rd1 mice, and C57BL/6 mice were maintained and bred in the animal facility of the School of Ophthalmology and Optometry at Wenzhou Medical University. All experiments were carried out in accordance with the Association for Research on Vison and Ophthalmology's statement on the Use of Animals in Ophthalmic and Vision Research and were approved by the Institutional Animal Care and Use Committee of Wenzhou Medical University. The mice were given free access to food and water under an environmental light intensity of 18 Lux on a 12-h dark/light cycle.

Generation of the DKO Mice. A conventional knockout strategy was applied to generate the miR-183/96–depleted mice. The vector RV-miR-183/96-Loxp (17.278 kb) was constructed to replace a 2.085-kb region flanking pre–miR-183 and pre–miR-96. More details are provided in *SI Appendix*.

Immunohistochemistry. Immunostaining of cryosectioned samples was used to compare the morphological changes in the retinas of DKO mice and controls, as described in *SI Appendix*.

RNA Isolation, qRT-PCR, and RNA-seq. Both eyes of a mouse were extirpated to prepare total RNA. qRT-PCR was performed using standard protocols (*SI Appendix*). For RNA-seq, a minimum of 4 μg of total RNA obtained from

mouse retina at P7 and P120 was used to establish indexed Illumina libraries according to the manufacturer's protocol. Sequencing was performed on the Illumina HiSeq 2000 platform (33, 34).

Western Blot Analysis. Extracted proteins from the retinas were separated by SDS/PAGE and electrotransferred onto a nitrocellulose membrane. The membranes were incubated with primary antibodies against Slc6a6 and Gapdh, followed by incubation with the corresponding secondary antibodies (*SI Appendix*).

ELISA. Isolated retinas were homogenized, and the supernatants were collected and analyzed according to the manufacturer's instructions. Samples and reference standards were loaded in a 96-well plate and then incubated with secondary antibody and working solution for 60 min in the dark. The plate was washed five times in washing buffer, then substrate was added and allowed to react for 30 min in the dark. After addition of a stopping solution, absorbance at 450 nm was recorded with a microplate reader.

Luciferase Assay and Transfection. For the luciferase assay, luciferase reporter plasmids containing sequences of Slc6a6, Rnf217, Dmxl1, and Med1 were constructed to validate potential miRNA targets. The psiCHECK-2 vector reporter plasmid containing the experimental luciferase gene as well as the firefly luciferase gene was used to normalize transfection efficiency. Luciferase signals were detected at 48 h posttransfection. The values were normalized to those of the NC control, and the assays were conducted in triplicate. Details are provided in *SI Appendix*.

AAV2/8-Mediated miR-183/96 and Slc6a6 Overexpression and Knockdown. To generate AAV2/8-mmu-miR-183/96, the target sequence was cloned into the NheI and HindIII sites of a GV412 vector containing CMV bGlobin-EGFP-MCS. To generate AAV2/8-mmu-Slc6a6, the target sequence was cloned into the BamHI and NheI sites of a GV420 vector containing CMV bGlobin-MCS-3FLAG. To generate AAV2/8-mmu-Slc6a6 RNAi, the target sequence 5′-TAT-AACAAGTACAAGTATA-3′ was cloned into a GV472 vector containing U6-MCS-CMV bGlobin-mCherry-3FLAG. The AAV2/8-mediated empty vector containing CMV-bGlobin-EGFP served as the control. These procedures are described in more detail in *SI Appendix*. The inserted sequences were generated by PCR using the primers listed in *SI Appendix*, Table S4.

Subretinal AAV Delivery. WT mice at P30 were anesthetized using ketamine and xylazine. A small incision was created in the lens near the sclera with a sharp 30-gauge needle, and 1 μL (1×10^{12} TU/mL) of AAV-mmu-Slc6a6, AAV-mmu-miR-183, and AAV-mmu-miR-96 for OD and control vector for OS was injected slowly into the subretinal space using a blunt 5-μL Hamilton syringe held in a micromanipulator. All injections were performed bilaterally, with the control vector in the OS and the objective gene vectors in the OD.

ERG. DKO mice and age-matched WT controls were paired for full-field ERGs, which were conducted as described previously (33) (*SI Appendix*).

Fundus Photography, SD-OCT, and FFA. miR-183/96–depleted mice and their littermates were dilated and anesthetized as previously described (33). For each mouse, experiments were performed in the following order: fundus photography, SD-OCT, and FFA. Details are provided in *SI Appendix*.

Buried Food Pellet Test. The buried food pellet test was carried out as described previously (34). The latency of uncovering the food pellet by the mouse, defined as grabbing a pellet with the forepaws and/or teeth, was calculated as the interval between the time when the mouse was placed in the cage and the time when it reached the target. The mice were subjected to one trial per day. The test is described in more detail in *SI Appendix*.

ACKNOWLEDGMENTS. We thank Dr. Yuk Fai Leung for critical review and suggestions, and Xiao-Yun Wang, De-Fu Chen, Ru-Yi Han, Qi-Zhi Yan, Qing-Kai Ma, Mei-Xiao Shen, Dong-Qing Li, Sheng-Hai Huang, Feng-Feng Li, Jun-Gang Wang, and Wen-Li Deng for technical assistance. We also thank the specific pathogen free (SPF) animal facility at Wenzhou Medical University for supporting this project. This study was supported by the National Natural Science Foundation of China (Grants 81522014, to Z.-B.J., 81500741, to X.-J.C., and 81371059, to Z.-B.J.), the National Key Basic Research Program (Grant 2013CB967502, to Z.B.J.), and funded in part by the Zhejiang Provincial Natural Science Foundation of China (Grant LQ14B020005, to X.-J.C.), the Zhejiang Provincial Key Research and Development Program (Grant 2015C03029), the National Health and Family Planning Commission (Grant-in-Aid for Medical and Health Science 201472911, to Z.-B.J.), and the Wenzhou Science and Technology Innovation Team Project (Grant C20150004).

1. Lee RC, Feinbaum RL, Ambros V (1993) The *C. elegans* heterochronic gene lin-4 encodes small RNAs with antisense complementarity to lin-14. *Cell* 75:843–854.
2. Ambros V (2004) The functions of animal microRNAs. *Nature* 431:350–355.
3. Mukherji S, et al. (2011) MicroRNAs can generate thresholds in target gene expression. *Nat Genet* 43:854–859.
4. Lumayag S, et al. (2013) Inactivation of the microRNA-183/96/182 cluster results in syndromic retinal degeneration. *Proc Natl Acad Sci USA* 110:E507–E516.
5. Damiani D, et al. (2008) Dicer inactivation leads to progressive functional and structural degeneration of the mouse retina. *J Neurosci* 28:4878–4887.
6. Zhu Q, et al. (2011) Sponge transgenic mouse model reveals important roles for the microRNA-183 (miR-183)/96/182 cluster in postmitotic photoreceptors of the retina. *J Biol Chem* 286:31749–31760.
7. Busskamp V, et al. (2014) miRNAs 182 and 183 are necessary to maintain adult cone photoreceptor outer segments and visual function. *Neuron* 83:586–600.
8. Li H, Kloosterman W, Fekete DM (2010) MicroRNA-183 family members regulate sensorineural fates in the inner ear. *J Neurosci* 30:3254–3263.
9. Kuhn S, et al. (2011) miR-96 regulates the progression of differentiation in mammalian cochlear inner and outer hair cells. *Proc Natl Acad Sci USA* 108:2355–2360.
10. Lewis MA, et al. (2009) An ENU-induced mutation of miR-96 associated with progressive hearing loss in mice. *Nat Genet* 41:614–618.
11. Krol J, et al. (2015) A network comprising short and long noncoding RNAs and RNA helicase controls mouse retina architecture. *Nat Commun* 6:7305.
12. Ubhi K, et al. (2014) Widespread microRNA dysregulation in multiple system atrophy—disease-related alteration in miR-96. *Eur J Neurosci* 39:1026–1041.
13. Christensen ST, Voss JW, Teilmann SC, Lambert IH (2005) High expression of the taurine transporter TauT in primary cilia of NIH3T3 fibroblasts. *Cell Biol Int* 29:347–351.
14. Lobo MV, Alonso FJ, Latorre A, del Río RM (2001) Immunohistochemical localization of taurine in the rat ovary, oviduct, and uterus. *J Histochem Cytochem* 49:1133–1142.
15. Young TL, Matsuda T, Cepko CL (2005) The noncoding RNA taurine upregulated gene 1 is required for differentiation of the murine retina. *Curr Biol* 15:501–512.
16. Warskulat U, et al. (2007) Taurine deficiency and apoptosis: Findings from the taurine transporter knockout mouse. *Arch Biochem Biophys* 462:202–209.
17. Jin ZB, et al. (2009) Targeted deletion of miR-182, an abundant retinal microRNA. *Mol Vis* 15:523–533.
18. Zhao L, Ma W, Fariss RN, Wong WT (2011) Minocycline attenuates photoreceptor degeneration in a mouse model of subretinal hemorrhage microglial: Inhibition as a potential therapeutic strategy. *Am J Pathol* 179:1265–1277.
19. Arroba AI, Alvarez-Lindo N, van Rooijen N, de la Rosa EJ (2011) Microglia-mediated IGF-I neuroprotection in the rd10 mouse model of retinitis pigmentosa. *Invest Ophthalmol Vis Sci* 52:9124–9130.
20. Wang X, et al. (2017) Tamoxifen provides structural and functional rescue in murine models of photoreceptor degeneration. *J Neurosci* 37:3294–3310.
21. Peng B, et al. (2014) Suppression of microglial activation is neuroprotective in a mouse model of human retinitis pigmentosa. *J Neurosci* 34:8139–8150.
22. Sturman JA (1988) Taurine in development. *J Nutr* 118:1169–1176.
23. Hayes KC, Carey RE, Schmidt SY (1975) Retinal degeneration associated with taurine deficiency in the cat. *Science* 188:949–951.
24. Altshuler D, Lo Turco JJ, Rush J, Cepko C (1993) Taurine promotes the differentiation of a vertebrate retinal cell type in vitro. *Development* 119:1317–1328.
25. Sarfare S, et al. (2014) Overexpression of rod photoreceptor glutamic acid-rich protein 2 (GARP2) increases gain and slows recovery in mouse retina. *Cell Commun Signal* 12:67.
26. Chakraborty D, Conley SM, Nash Z, Ding XQ, Naash MI (2012) Overexpression of ROM-1 in the cone-dominant retina. *Adv Exp Med Biol* 723:633–639.
27. Tan E, et al. (2001) The relationship between opsin overexpression and photoreceptor degeneration. *Invest Ophthalmol Vis Sci* 42:589–600.
28. Peng GH, Chen S (2011) Active opsin loci adopt intrachromosomal loops that depend on the photoreceptor transcription factor network. *Proc Natl Acad Sci USA* 108:17821–17826.
29. Tran NM, et al. (2014) Mechanistically distinct mouse models for CRX-associated retinopathy. *PLoS Genet* 10:e1004111.
30. Wenngren BI, Anniko M (1989) Vestibular hair cell pathology in the dancer mouse mutant. *Acta Otolaryngol* 107:182–190.
31. Alagramam KN, Stahl JS, Jones SM, Pawlowski KS, Wright CG (2005) Characterization of vestibular dysfunction in the mouse model for Usher syndrome 1F. *J Assoc Res Otolaryngol* 6:106–118.
32. Nathan BP, Yost J, Litherland MT, Struble RG, Switzer PV (2004) Olfactory function in apoE knockout mice. *Behav Brain Res* 150:1–7.
33. Jin ZB, et al. (2014) SLC7A14 linked to autosomal recessive retinitis pigmentosa. *Nat Commun* 5:3517.
34. Umbarger MA, et al. (2014) Next-generation carrier screening. *Genet Med* 16:132–140.